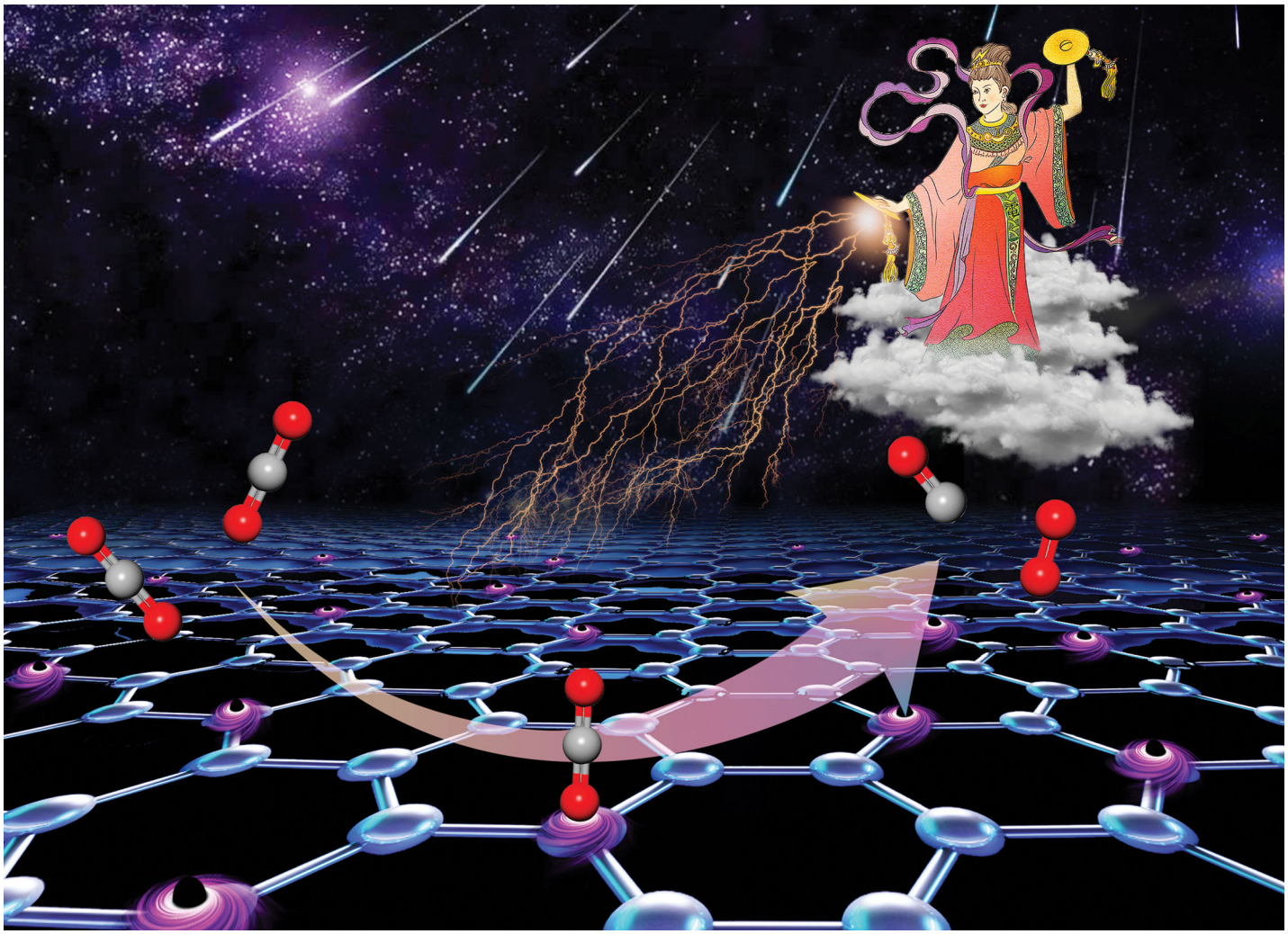

Showcasing research from Professor Li Wang's group at Dalian Maritime University, China and Professor Xin Tu's group at the University of Liverpool, UK

Plasma-enhanced direct conversion of CO_2 to CO over oxygen-deficient Mo-doped CeO_2

Plasma-catalytic direct splitting of CO_2 to CO over oxygen-deficient Mo-doped CeO_2 at ambient conditions was achieved. Developing new catalytic technologies involving plasma opens the door to unlocking the potential of using captured CO_2 to make valuable chemicals under mild conditions.

As featured in:

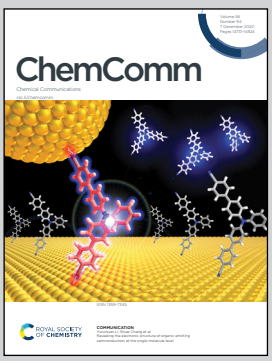

See Li Wang, Xin Tu *et al.*, *Chem. Commun.*, 2020, **56**, 14801.

ROYAL SOCIETY OF CHEMISTRY

rsc.li/chemcomm

Registered charity number: 207890

ChemComm

COMMUNICATION

View Article Online
View Journal | View Issue

Check for updates

Cite this: *Chem. Commun.*, 2020, **56**, 14801

Received 28th September 2020,
Accepted 6th November 2020

DOI: 10.1039/d0cc06514e

rsc.li/chemcomm

Open Access Article. Published on 09 November 2020. Downloaded on 1/15/2026 7:31:08 AM.
This article is licensed under a Creative Commons Attribution 3.0 Unported Licence.

Plasma-enhanced direct conversion of CO_2 to CO over oxygen-deficient Mo-doped CeO_2†

Li Wang, *[a] Xiaomin Du,[a] Yanhui Yi,[b] Hongyang Wang,[a] Masaud Gul,[a] Yimin Zhu[a] and Xin Tu *[c]

Plasma CO_2 splitting to CO over oxygen-deficient Mo-doped CeO_2 under mild conditions was investigated for the first time, showing ~20 times higher CO_2 conversion compared to pure CeO_2, which can be attributed to the increased oxygen vacancies (V_O) and the formation of Ce^{3+}–V_O–Mo on the catalyst surface. Importantly, V_O sites showed excellent catalytic stability.

Converting CO_2 to value-added fuels and chemicals has been considered as a promising route in CO_2 utilization. Significant efforts have been devoted to the chemical transformation of CO_2, including thermal catalysis,[1] photocatalysis,[2,3] electrocatalysis,[4,5] and plasma catalysis.[6,7] Direct splitting of CO_2 to CO without using any reductant is attractive for CO_2 conversion, as CO is an important chemical feedstock for the synthesis of a range of chemicals and fuels. However, this reaction has to overcome a strong thermodynamic barrier ($CO_2 \rightarrow CO + 1/2O_2$, ΔH_{298K} = 280 kJ mol^{-1} = 2.9 eV $molecule^{-1}$) to break the C=O bond, since CO_2 is very stable. Ultrahigh temperatures (2000 K) are often required to activate CO_2 (Fig. S1, ESI†).

In recent years, using non-thermal plasmas (NTPs) for the activation of inert molecules with strong chemical bonds (*e.g.*, CO_2, CH_4 and N_2) under mild conditions has attracted significant interest, including CO_2 reforming with CH_4 to oxygenates,[8,9] CO_2 hydrogenation to methanol,[10] and ammonia synthesis.[11] NTP is rich in energetic electrons with a typical energy of 1–10 eV, which is sufficient to activate reactants into chemically reactive species, enabling thermodynamically unfavorable reactions (*e.g.* CO_2 splitting) to proceed at ambient conditions.

Up until now, studies on plasma CO_2 splitting to CO mainly focused on the optimization of operating parameters,[12–16] and only a few catalysts (*e.g.*, Ni/SiO_2, NiO/TiO_2 and Rh/TiO_2) have been evaluated (Table S1, ESI†).[17–20] Recently, surface oxygen vacancies (V_O) have been suggested to be the active sites in plasma-catalytic CO_2 splitting to CO. Mei *et al.* reported that higher CO_2 conversion was achieved when coupling plasma with $BaTiO_3$, which can be explained by the formation of more V_O sites on the surfaces of $BaTiO_3$ compared with TiO_2.[20] Chen *et al.* found the V_O on Ni/TiO_2 contributed to the enhanced CO_2 dissociation.[18] In fact, the coupling of catalysts and plasma is a promising strategy to improve CO_2 conversion and energy efficiency. However, the knowledge in selection of appropriate catalysts for highly efficient CO_2 splitting to CO using NTP was still very limited until now.

Herein, CO_2 splitting to CO over M-doped CeO_2 catalysts (M = Fe, Co, Ni, Cu, Cr, V, Mn or Mo) has been carried out in a dielectric barrier discharge (DBD) reactor (Fig. S2–S5, ESI†). CeO_2 not only serves as a support to anchor and disperse the metal oxide particles but also generates V_O active sites through the interaction with metal oxides. Significant differences were observed among the M-doped CeO_2 catalysts in terms of CO_2 conversion, and the Mo-doped CeO_2 exhibited the best activity in CO_2 conversion (Fig. S3, ESI†). Therefore, Mo-doped CeO_2 has been selected for further studies.

Comprehensive catalyst characterization was carried out to understand the physicochemical properties of Mo-doped CeO_2. As shown in Fig. 1, the X-ray diffraction (XRD) pattern of CeO_2 exhibits characteristic peaks of a cubic fluorite phase (JCPDS, 34-0394). For Mo-doped CeO_2, small peaks of α-MoO_3 (JCPDS, 05-0508) and Mo_4O_{11} (JCPDS, 05-0337) are observed, revealing the coexistence of Mo(VI) and Mo(V) species. Notably, the characteristic peaks of CeO_2 downshift compared to pure CeO_2, which suggests that Mo doping leads to the expansion of the CeO_2 unit cell. Usually, inserting Mo ions into CeO_2 induces shrinkage of the CeO_2 unit cell since the radius of Mo ions is much smaller than that of Ce ions, resulting in upshifting of CeO_2 peaks, rather than downshifting. Thus, Mo ions do not insert into the CeO_2 unit cell, and there might be other reasons responsible for this downshift. X-ray photoelectron spectroscopy

[a] *College of Environmental Sciences and Engineering, Dalian Maritime University, Dalian, 116026, P. R. China. E-mail: liwang@dlmu.edu.cn*
[b] *State Key Laboratory of Fine Chemicals, School of Chemical Engineering, Dalian University of Technology, Dalian 116012, P. R. China*
[c] *Department of Electrical Engineering and Electronics, University of Liverpool, Liverpool, L69 3GJ, UK. E-mail: xin.tu@liv.ac.uk*

† Electronic supplementary information (ESI) available. See DOI: 10.1039/d0cc06514e

Open Access Article. Published on 09 November 2020. Downloaded on 1/15/2026 7:31:08 AM.
This article is licensed under a Creative Commons Attribution 3.0 Unported Licence.

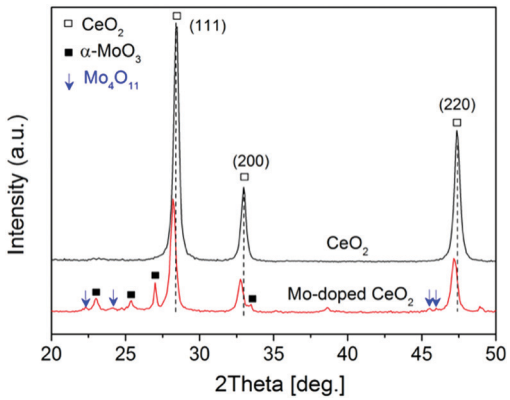

Fig. 1 XRD patterns of CeO_2 and as-prepared Mo-doped CeO_2.

(XPS) was employed to analyze surface properties of Mo-doped CeO_2. The deconvoluted Ce 3d XPS spectra are presented in Fig. 2(a). The peaks labeled as v, v″, v‴ and u, u″, u‴ are assigned to $3d_{5/2}$ and $3d_{3/2}$ electrons of Ce^{4+}, respectively, while the peaks of v′, u′ and v_o, u_o correspond to $3d_{5/2}$ and $3d_{3/2}$ electrons of Ce^{3+}, respectively.[21] Clearly, Ce^{3+} exists in CeO_2 and Mo-doped CeO_2, suggesting the formation of V_O in both samples. More importantly, the proportion of Ce^{3+} in Mo-doped CeO_2 is 40.2%, higher than that in CeO_2 (30.0%) (Fig. S6 and S7, ESI†). This finding suggests that Mo doping induces partial transformation of Ce^{4+} to Ce^{3+} and creates more V_O on Mo-doped CeO_2. As reconfirmed by the O 1s XPS spectra in Fig. 2(b) and Fig. S6 (ESI†), a higher surface V_O (30.4%) is achieved in the Mo-doped CeO_2 in comparison to pure CeO_2 (21.0%). Furthermore, the transformation of Ce^{4+} to Ce^{3+} leads to the expansion of the CeO_2 unit cell since the ion radius of Ce^{3+} (1.23 Å) is higher than that of Ce^{4+} (0.97 Å),[22] which explains the reason for the downshifting of CeO_2 peaks in Fig. 1. More interestingly, the binding energies of Ce 3d shift significantly towards higher values after Mo doping, revealing that the electron density of the surface CeO_2 species is lower in Mo-doped CeO_2 compared with pure CeO_2, which might be induced by the electron transfer from Ce to Mo, due to the higher electronegativity of Mo. These results suggest different properties of V_O sites in the form of Ce^{3+}–V_O in CeO_2 and Ce^{3+}–V_O–Mo in Mo-doped CeO_2, as well as the strong interaction between Mo and CeO_2, which agrees with the results of H_2-temperature programmed reduction (H_2-TPR), scanning electron microscopy (SEM) and transmission electron microscopy (TEM) (Fig. S8–S11, ESI†). Fig. 2(c) shows the deconvoluted Mo 3d spectra, in which the Mo-doped CeO_2 sample exhibits typical doublet peaks of Mo^{6+} with an energy gap of *ca.* 3.1 eV, indicating the formation of MoO_3 in Mo-doped CeO_2.[23] The two smaller peaks observed, however, are identified to be $3d_{3/2}$ and $3d_{5/2}$ electrons of Mo(v), demonstrating the formation of the non-stoichiometric MoO_{3-x},[23] which is consistent with the Mo_4O_{11} species confirmed by the XRD analysis (Fig. 1). Fig. 2(d) shows the Raman spectra of CeO_2 and Mo-doped CeO_2. For pure CeO_2, the intense band at 465 cm^{-1} is well-indexed to the typical F2g modes of a cubic CeO_2 fluorite structure, and the weak bands at 262, 597 and 1171 cm^{-1} are assigned to V_O, reconfirming the XPS results in Fig. 2(a and b).[23] For Mo-doped CeO_2, the emerging Raman bands at 673, 824 and 997 cm^{-1} are assigned to MoO_3 crystallites.[24] However, the band at 955 cm^{-1} is associated with Mo suboxides (MoO_{3-x}).[24,25] These results indicate that the valence state of Mo in suboxides is Mo^{5+}. Moreover, the presence of Mo^{5+} and Ce^{3+} indicates that more V_O sites are created through the strong interaction between Mo and CeO_2, as well as the calcining atmosphere with deficient oxygen and rich energetic Ar species, which agrees with the results reported by Chen *et al.*[18]

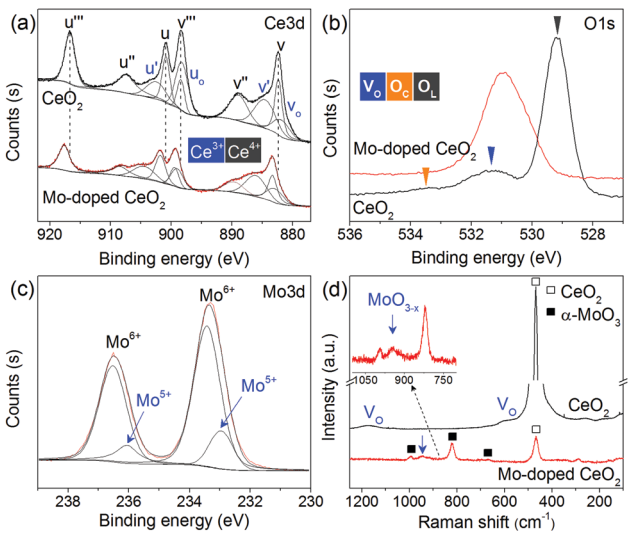

Fig. 2 XPS and Raman spectra of CeO_2 and as-prepared Mo-doped CeO_2 (a) Ce 3d, (b) O 1s, (c) Mo 3d and (d) Raman spectra (V_O, O_C and O_L represent oxygen vacancy, chemisorbed oxygen species and oxygen lattice, respectively).

Fig. 3 shows the effect of different operating conditions on CO_2 conversion. Clearly, no reaction occurred without plasma (catalyst only, 400 °C). The conversion of CO_2 was 3.8% in the plasma reaction without a catalyst (plasma only). In the plasma reaction coupled with pure CeO_2, the CO_2 conversion dropped to 1.2%, which suggests that pure CeO_2 is unfavorable for CO_2 splitting to CO despite CeO_2 being O-deficient. Using Mo-doped

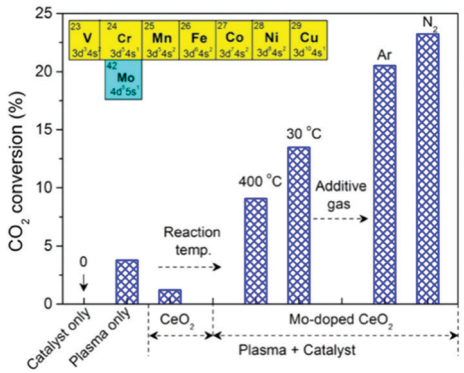

Fig. 3 Effect of reaction temperature and additive gas on CO_2 conversion (CO_2 flow rate 40 ml min^{-1}, SEI 20 kJ L^{-1}, molar ratio 4 : 1 and 30 °C for CO_2/Ar and CO_2/N_2; catalyst only 400 °C).

This journal is © The Royal Society of Chemistry 2020

Open Access Article. Published on 09 November 2020. Downloaded on 1/15/2026 7:31:08 AM.
This article is licensed under a Creative Commons Attribution 3.0 Unported Licence.

CeO_2 instead of CeO_2, however, results in a significant increase of CO_2 conversion by a factor of 9 at 400 °C. In addition, the Mo-doped CeO_2 showed stable CO_2 conversion for at least 10 h (Fig. S12, ESI†). Interestingly, the reaction performance can be further improved by using a lower reaction temperature (30 °C) and an additive gas (Ar or N_2). This promotional effect was more pronounced when adding N_2. The highest CO_2 conversion of 23.2% and energy efficiency of 14.3% were achieved in the plasma splitting of CO_2 with N_2 addition over Mo-doped CeO_2 at 30 °C (Table S1, ESI†), while the corresponding formation rate of CO and O_2 was 24.9 mmol h^{-1} and 12.4 mmol h^{-1}, respectively (Table S2, ESI†). The optimal energy efficiency achieved in this study is comparable to that reported in previous works (Table S1, ESI†).

Regarding surface reactions, the improved activity over Mo-doped CeO_2, on one hand, is mainly attributed to the increased formation of V_O (Fig. 2 and Fig. S6, ESI†), since V_O serve as adsorption centers for CO_2 dissociative adsorption,[17,26] *i.e.*, $CO_2 + V_O \rightarrow O_L/O_C + CO$. On the other hand, the promoted performance originates from the different properties of V_O in the forms of Ce^{3+}–V_O and Ce^{3+}–V_O–Mo due to strong interaction between Mo and CeO_2 and the higher electronegativity of Mo compared with Ce (Fig. 1, 2 and Fig. S8, ESI†), which leads to a stronger binding strength of CO_2 with the V_O of Ce^{3+}–V_O–Mo. As discussed above, V_O is the active site for CO_2 activation; thus, the stability of V_O greatly influences the subsequent catalytic cycle. It is well recognized that oxygen can be produced in plasma CO_2 splitting, and the produced O species could poison the catalyst through filling V_O sites to form stable lattice oxygen species, resulting in termination of the catalytic cycle.

Therefore, the spent Mo-doped CeO_2 catalysts were further characterized by XPS, Raman, XRD and H_2-TPR (Fig. 4). Interestingly, compared with the fresh catalyst, the spent Mo-doped CeO_2 catalysts show an increased amount of Ce^{3+} and MoO_{3-x}, which can be confirmed by the higher intensities of Ce^{3+} peaks and the Raman band at ~950 cm^{-1} in Fig. 4(a and b), respectively. The enhancement effect is more pronounced for the catalyst used at 400 °C. Correspondingly, more V_O sites were created in the high-temperature reaction (Table S3, ESI†). In addition, the color of the catalyst changed from gray/blue (MoO_{3-x}) to yellow (MoO_{3-y}) with $x > y$ after the reaction at 30 °C, while no visible changes were observed on the phase structure of Mo-doped CeO_2 before and after the reaction (30 °C), as shown in Fig. 4(c). These results indicate that some O atoms from CO_2 splitting are adsorbed onto the catalyst, as seen by the slightly increased H_2 consumption in Fig. 4(d). Even so, the V_O concentration of Mo-doped CeO_2 used at 30 °C remained at a similar level with that of the fresh sample (Table S3, ESI†). These findings suggest that V_O-rich Mo-doped CeO_2 is stable after the plasma reaction, and high-temperature reactions facilitate the formation and recovery of V_O sites, resulting from accelerating recombinative desorption of adsorbed O atoms.[27]

In addition to surface reactions, gas-phase reactions also play a crucial role in the plasma-catalytic process. In a pure CO_2 DBD, CO_2 splitting to CO mainly proceeds through the electron impact dissociation of CO_2 ($CO_2 + e \rightarrow CO + O + e$), which can be confirmed by plasma chemical kinetic modeling,[28] as well as the formation of CO bands and O atomic lines detected by optical emission spectra of CO_2 DBD (Fig. 5(a)). As shown in Fig. 5(a), the presence of strong N_2 ($C^3\Pi_u \rightarrow B^3\Pi_g$, $B^3\Pi_g \rightarrow A^3\Sigma_u^+$) molecular bands and Ar atomic lines suggests the formation of excited nitrogen species (N_2*) and metastable Ar species (Ar*).[29,30] These species create an additional reaction route for CO_2 dissociation (N_2* (or Ar*) + $CO_2 \rightarrow CO + O + N_2$ (or Ar)), supported by the increased intensity of O atomic lines and CO bands when adding N_2 or Ar, which contributes to the enhanced CO_2 conversion. Furthermore, 150 ppm NO_x was detected by Fourier transform infrared (FTIR) in the case of N_2 addition (Fig. S13, ESI†), revealing that N_2 can be regarded as an alternative scavenger of O species.[12] The elimination of partial O species can effectively limit the reverse reaction, *i.e.*, $O + CO + M \rightarrow CO_2 + M$, and thus enhance the CO_2 conversion. This could explain why adding N_2 has a stronger promotion on the CO_2 conversion compared with Ar.

Interaction between reactive species in the gas phase and catalyst is also crucial in plasma-catalytic reactions.[31] Compared to plasma only, packing Mo-doped CeO_2 into the

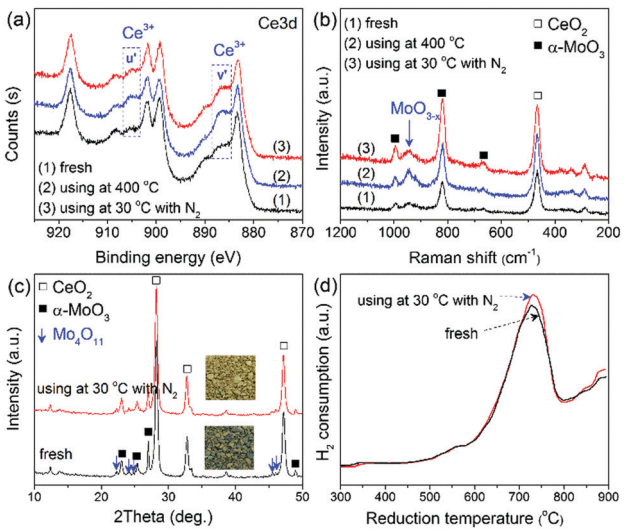

Fig. 4 (a) XPS spectra, (b) Raman spectra, (c) XRD patterns, (d) H_2-TPR profiles of Mo-doped CeO_2 before and after reaction.

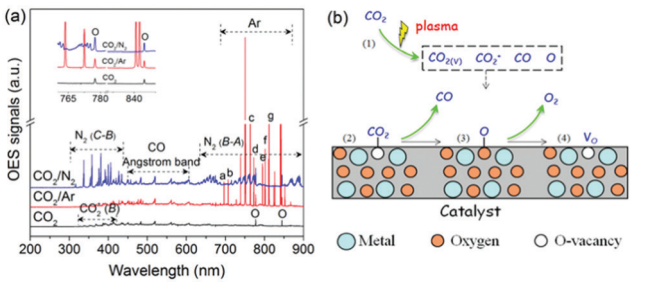

Fig. 5 (a) Emission spectra of CO_2 plasma, (b) possible pathways of plasma-catalytic CO_2 splitting over V_O-rich catalyst.

Open Access Article. Published on 09 November 2020. Downloaded on 1/15/2026 7:31:08 AM.
This article is licensed under a Creative Commons Attribution 3.0 Unported Licence.

discharge zone decreased the current (Fig. S14, ESI†), lowering the contribution of the gas-phase reactions. In this case, the CO_2 conversion, however, was still improved, which might be attributed to the interaction between active species and V_O-rich Mo-doped CeO_2, accelerating V_O recovery. Therefore, a possible reaction mechanism is proposed in Fig. 5(b). Firstly, CO_2 is activated to species of CO_2^+, $CO_{2(v)}$, CO and O radicals as shown in Fig. 5(a) (step 1). Then, the energetic CO_2-species are adsorbed on the V_O sites to decrease their internal energy (step 2). After that, the V_O sites have the potential to grasp the O atom of the adsorbed CO_2 molecule, which weakens the C═O bond, producing adsorbed CO and O (step 3). Subsequently, the adsorbed CO desorbs as the final CO product. While the adsorbed O mainly desorbs from V_O sites in the form of O_2 through reacting with the active O radicals produced in the gas phase ($O_g + O_{ad}–V_O \rightarrow O_{2,g} + V_O$), *i.e.*, Eley–Rideal (E–R) mechanism. Meanwhile, V_O sites recover completing the catalytic cycle (step 4). Using isotope trace analysis, we demonstrated the desorption of N_{ad} through an E–R reaction in plasma-catalytic NH_3 decomposition.[31] Therefore, the desorption of O_{ad} through E–R reaction is also expected. Note that, too strong of a CO_2–V_O bond makes it easy to split the CO_2 molecule, but the corresponding desorption of adsorbed O is difficult. By contrast, too weak of a CO_2–V_O bond means it could be hard to split CO_2, although the adsorbed O can easily desorb from the catalyst surface. Therefore, a catalyst with a proper binding strength between V_O sites and CO_2 benefits the conversion of CO_2 and favors the catalytic cycle.

In conclusion, plasma-catalytic CO_2 splitting over M-doped CeO_2 catalysts (M = Fe, Co, Ni, Cu, Cr, V, Mn or Mo) has been investigated. Mo-doped CeO_2 exhibited the best activity; this is attributed to the increased oxygen vacancies created by strong interaction between Mo and CeO_2, as well as the calcining atmosphere being oxygen-deficient and rich in Ar metastable species. Furthermore, oxygen vacancies were stable during the reaction, which is ascribed to the interaction between active O produced in the gas phase and the adsorbed O on the oxygen vacancy site, resulting in desorbing as O_2 molecules and recovering oxygen vacancy sites. These findings suggest that introducing proper doping on CeO_2 offers a potential route to tune properties of oxygen vacancy in CeO_2. Additionally, adding N_2 and Ar into the plasma process enhanced the CO_2 conversion, especially when adding N_2. This promotional effect is mainly attributed to the new reaction routes induced by the presence of metastable species. We found that N_2 can be used as an O scavenger to forward the chemical equilibrium and inhibit the reverse reaction to form CO_2.

This work was financially supported by the NSFC (No. 21908016), the Liaoning Natural Science Foundation (No. 2019-MS-023 and 2018011143-301), the key Science and Technology Project List of Ministry of Transport of the People's Republic of China (No. 2018-ZD4-027). X. Tu acknowledges the funding from the European Union's Horizon 2020 research and innovation programme under the Marie Sklodowska-Curie grant agreement no. 823745 and the State Key Laboratory of Electrical Insulation and Power Equipment at Xi'an Jiaotong University (No. EIPE19207), China.

Conflicts of interest

There are no conflicts to declare.

Notes and references

1 J. Zhong, X. Yang, Z. Wu, B. Liang, Y. Huang and T. Zhang, *Chem. Soc. Rev.*, 2020, **49**, 1385.
2 S. Xie, Q. Zhang, G. Liu and Y. Wang, *Chem. Commun.*, 2016, **52**, 35.
3 Y. Lan, Y. Xie, J. Chen, Z. Hu and D. Cui, *Chem. Commun.*, 2019, **55**, 8068.
4 D. U. Nielsen, X. Hu, K. Daasbjerg and T. Skrydstrup, *Nat. Catal.*, 2018, **1**, 244.
5 X. Yuan, Y. Luo, B. Zhang, C. Dong, J. Lei, F. Yi, T. Duan, W. Zhu and R. He, *Chem. Commun.*, 2020, **56**, 4212.
6 A. George, B. Shen, M. Craven, Y. Wang, D. Kang, C. Wu and X. Tu, *Renewable Sustainable Energy Rev.*, 2021, **135**, 109702.
7 A. Bogaerts, X. Tu, J. C. Whitehead, G. Centi, L. Lefferts, O. Guaitella, F. A. Jury, H. H. Kim, A. B. Murphy, W. F. Schneider, T. Nozaki, J. C. Hicks, A. Rousseau, F. Thevenet, A. Khacef and M. Carreon, *J. Phys. D: Appl. Phys.*, 2020, **53**, 443001.
8 D. Li, V. Rohani, F. Fabry, A. P. Ramaswamy, M. Sennour and L. Fulcheri, *Appl. Catal., B*, 2020, **261**, 118228.
9 L. Wang, Y. Yi, C. Wu, H. Guo and X. Tu, *Angew. Chem., Int. Ed.*, 2017, **56**, 13679.
10 L. Wang, Y. Yi, H. Guo and X. Tu, *ACS Catal.*, 2018, **8**, 90.
11 Y. Wang, M. Craven, X. Yu, J. Ding, P. Bryant, J. Huang and X. Tu, *ACS Catal.*, 2019, **9**, 10780.
12 R. Snoeckx, S. Heijkers, K. V. Wesenbeeck, S. Lenaerts and A. Bogaerts, *Energy Environ. Sci.*, 2016, **9**, 999.
13 D. Mei and X. Tu, *J. CO_2 Util.*, 2017, **19**, 68.
14 D. Mei, X. Zhu, Y. He, J. D. Yan and X. Tu, *Plasma Sources Sci. Technol.*, 2015, **24**, 015011.
15 K. V. Laer and A. Bogaerts, *Plasma Processes Polym.*, 2017, **14**, 1600129.
16 D. Ray and C. Subrahmanyam, *RSC Adv.*, 2016, **6**, 39492.
17 K. Zhang, G. Zhang, X. Liu, A. N. Phan and K. Luo, *Ind. Eng. Chem. Res.*, 2017, **56**, 3204.
18 G. Chen, V. Georgieva, T. Godfroid, R. Snyders and M. Delplancke-Ogletree, *Appl. Catal., B*, 2016, **190**, 115.
19 L. F. Spencer and A. D. Gallimore, *Plasma Sources Sci. Technol.*, 2013, **22**, 015019.
20 D. Mei, X. Zhu, C. Wu, B. Ashford, P. T. William and X. Tu, *Appl. Catal., B*, 2016, **182**, 525.
21 C. Anandan and P. Bera, *Appl. Surf. Sci.*, 2013, **283**, 297.
22 W. Wang, Q. Zhu, F. Qin, Q. Dai and X. Wang, *Chem. Eng. J.*, 2018, **333**, 226.
23 K. Murugappan, E. M. Anderson, D. Teschner, T. E. Jones, K. Skorupska and Y. Román-Leshkov, *Nat. Catal.*, 2018, **1**, 960.
24 B. Liu, L. France, C. Wu, Z. Jiang, V. L. Kuznetsov, H. A. Al-Megren, M. Al-Kinany, S. A. Aldrees, T. Xiao and P. P. Edwards, *Chem. Sci.*, 2015, **6**, 5152.
25 K. Chen, S. Xie, A. T. Bell and E. Iglesia, *J. Catal.*, 2001, **198**, 232.
26 L. Liang, X. Li, Y. Sun, Y. Tan, X. Jiao, H. Ju, Z. Qi, J. Zhu and Y. Xie, *Joule*, 2018, **2**, 1004.
27 P. G. Dickens and M. B. Sutcliffe, *Trans. Faraday Soc.*, 1964, **60**, 1272.
28 R. Aerts, T. Martens and A. Bogaerts, *J. Phys. Chem. C*, 2012, **116**, 23257.
29 Y. Horikawa, T. Hayashi and K. Sasaki, *Jpn. J. Appl. Phys.*, 2012, **51**, 126301.
30 J. B. Boffard, G. A. Piech, M. F. Gehrke, L. W. Anderson and C. C. Lin, *Phys. Rev. A: At., Mol., Opt. Phys.*, 1999, **59**, 2749.
31 L. Wang, Y. Zhao, C. Y. Liu, W. M. Gong and H. C. Guo, *Chem. Commun.*, 2013, **49**, 3787.

 This journal is © The Royal Society of Chemistry 2020